Dynamics of precise ethylene ionomers containing ionic liquid functionality

Dynamics of Precise Ethylene Ionomers Containing Ionic Liquid Functionality

U Hyeok Choi,[1,2] L. Robert Middleton,[3] Michelina Soccio,[1] C. Francisco Buitrago,[4] Brian S. Aitken,[5] Hanqing Masser,[1,#] Kenneth B. Wagener,[5] Karen I. Winey,[3,4] and James Runt*[1]

[1]Department of Materials Science and Engineering, The Pennsylvania State University, University Park, Pennsylvania 16802, United States

[2]Functional Composites Department, Korea Institute of Materials Science, Changwon, 642-831, Korea

[3]Department of Materials Science and Engineering, University of Pennsylvania, Philadelphia, Pennsylvania 19104, United States

[4]Department of Chemical and Biomolecular Engineering, University of Pennsylvania, Philadelphia, Pennsylvania 19104, United States

[5]George and Josephine Butler Polymer Research Laboratory, Department of Chemistry, University of Florida, Gainesville, Florida 32611, United States

[#]Present address: The Dow Chemical Company, Spring House, PA 19477

* Correspondence to: James Runt (runt@matse.psu.edu)

Abstract

This paper presents the first findings on the molecular dynamics of the remarkable new class of linear and precisely functionalized ethylene copolymers. Specifically, we utilize broadband dielectric relaxation spectroscopy to investigate the molecular dynamics of linear polyethylene (PE)-based ionomers containing 1-methylimidazolium bromide (**ImBr**) pendants on exactly every 9th, 15th, or 21st carbon atom, along with one pseudorandom analogue. We also employed FTIR spectroscopy to provide insight on local ionic interactions and the nature of the ordering of the ethylene spacers between pendants. Prior X-ray scattering experiments revealed that the polar ionic groups in these ionomers self-assemble into microphase-separated aggregates dispersed throughout the nonpolar PE matrix. We focus primarily on the dynamics of the segmental relaxations, which are significantly slowed down compared to linear PE due to ion aggregation. Relaxation times depend on composition, the presence of crystallinity, and microphase-separated morphologies. Segmental relaxation strengths are much lower than predicted by the Onsager theory for mobile isolated dipoles, but much higher than linear PE demonstrating that at least some **ImBr** pendants participate in the segmental process. Analysis of the relaxation strengths using the Kirkwood g correlation factor demonstrates that ca. 10 – 40% of the **ImBr** ion dipoles (depending on copolymer composition and temperature) participate in the segmental motions of the precise ionomers under study, with the remainder immobilized or having net anti-parallel arrangements in ion aggregates.

1. Introduction

A molecular-level understanding of the dynamics of ionomers, polymers containing ionic functionality, is of considerable importance from both fundamental and applied points of view. The presence of ionic groups in, or pendant to, polymer chains is well known to significantly modify thermal, mechanical, and charge transport properties of the parent polymer due to various ionic interactions.[1,2] As a result of the low dielectric constant of most organic polymers, ion dipoles tend to self-assemble into microphase-separated domains. Consequently, much of the fundamental research conducted on these materials has been devoted to determination of the structure of ion aggregates and the correlation between structure and the resulting properties.[3] Ionomers have been used commercially as separators, packaging materials and in molding applications,[4] and in recent years have been considered as candidate materials for energy storage devices (batteries and supercapacitors), in energy conversion (fuel cells) and for other electroactive materials applications.[5,6]

Ionomers derived from copolymers of ethylene and methacrylic acid (MAA) have been well known since the 1960's, principally due to their versatile mechanical properties and chemical stability.[2-4,7] Since these materials have relatively low MAA content and MAA units are randomly placed in the highly-branched polyethylene (PE) chains, long PE sequences exist and are capable of crystallization. The microstructure – property – processing relationships of these traditional ionomers have been the subject of many previous publications.[8-18]

The relatively recent discovery of a synthetic route for creating ethylene copolymers with precisely placed acid functionality along the chain has led to a remarkable new class of highly regular acid-functionalized (and cation-neutralized) ethylene copolymers.[19-24] Extensive morphological characterization of a growing number of precise acid copolymers and their ionomers has uncovered morphologies with considerably sharper X-ray scattering features (i.e., much less environmental heterogeneity) and unprecedented uniformity.[20,25-28] Computer simulations have also been used to explore the ionic aggregation in PE-based precise ionomers and compact isolated aggregates, branched string-like aggregates, and percolated structures have been observed.[24,29-32] However, despite recent advances in our understanding of the microphase-separated morphology of these unique copolymers and ionomers, there have been to date no reports on their molecular dynamics.

Herein, we focus on the investigation of polymer and ion dynamics of three precise (and one pseudorandom) PE-based ionomers, using dielectric relaxation spectroscopy (DRS). In a recent publication, acyclic diene metathesis (ADMET) polymerization in combination with post-polymerization functionalization was used to successfully produce linear high molecular weight PE with 1-methylimidazolium bromide (**ImBr**) units precisely substituted on every 9th, 15th, or 21st carbons along the chain, as shown in Figure 1.[33] Dielectric spectroscopy is a particularly powerful tool for investigating the impact of associating ion pairs or aggregates on the motion of chain segments and substituent groups, over a broad range of frequencies and temperatures. In addition, the non-polar ethylene portions of the ionomers exhibit very low dielectric loss, allowing one

to focus on the molecular motions of the ionic functionality. As there is an intimate connection between phase separated microstructure and molecular dynamics, the dynamics of the precise ionomers cannot be well understood without microstructural insight. Consequently, our dielectric spectroscopy investigation is complemented by X-ray scattering and DSC measurements, as well as insight on local ionic interactions and ethylene spacer ordering from Fourier transform infrared spectroscopy.

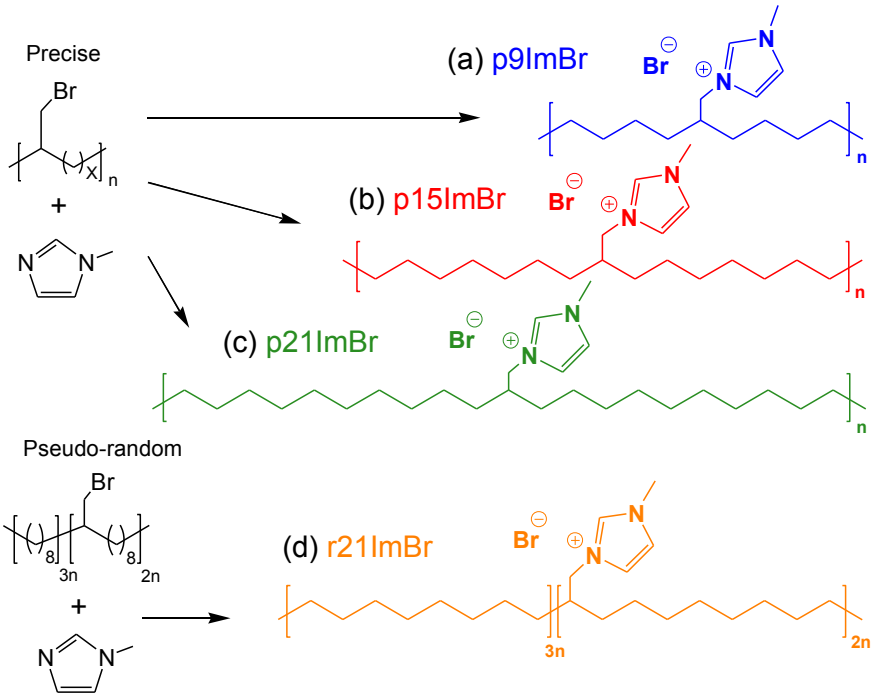

Figure 1. The chemical structures of three polyethylene-based precise ionomers containing 1-methylimidazolium bromide groups on exactly every (a) 9th (**p9ImBr**), (b) 15th (**p15ImBr**), and (c) 21st (**p21ImBr**) carbon.[33] The findings on these precise ionomers are also compared with (d) a pseudorandom analogue (**r21ImBr**) that is compositionally identical to its precise counterpart (**p21ImBr**).[33]

2. Experimental

Figures 1a-c show the molecular structures of the polyethylene (PE)-based ionomers containing 1-methylimidazolium bromide (**ImBr**) groups on exactly every 9th (referred to as **p9ImBr**), 15th (**p15ImBr**), and 21st (**p21ImBr**) carbon atom: the letter **p** indicates precise placement of ionic pendant groups along the polymer chain. These are linear high molecular weight materials with a polydispersity index of ~2.[33] The findings on these precise ionomers are also compared with those from one pseudorandom analogue (**r21ImBr**; its molecular structure is shown in Figure 1d). The letter **r** indicates pseudorandom substitution and the number 21 denotes that, on average, there is one pendant per 21 carbon atoms, which makes this ionomer compositionally identical to its precise counterpart (**p21ImBr**).

Sample Preparation. For this study, the ionomer samples were prepared in the following manner. Films for FTIR, DSC, X-ray scattering, and dielectric measurements were melt-pressed at 150 °C for 20 min in a Carver 4122 hot press. Note that the thermal transitions (T_g, T_m) of all the ionomers are well below 150 °C (see Table 1). The films were then subjected to rapid cooling (~15 °C/min) via a heat exchanger using tap water, and aged at room temperature in a vacuum dessicator for at least 3 days before data collection. Samples used in all experiments have the identical thermal history.

Fourier Transform Infrared Spectroscopy (FTIR). FTIR spectra were determined using a Nicolet 6700 FTIR spectrometer (Thermo Scientific) equipped with a diamond attenuated

total reflectance (ATR) cell. The spectra were signal averaged from 200 scans with a resolution of 2 cm^{-1}.

Thermal Characterization. Differential scanning calorimetry (DSC) results were obtained on a TA Instruments Q2000 differential scanning calorimeter, with temperature and enthalpy calibrated using an indium standard. Samples weighed approximately 5 – 10 mg, and the thermograms were measured at a heating rate of 10 K/min under a helium purge. TA Instruments Universal Analysis 2000 Software was used to identify the phase transitions (T_g, T_m and ΔH_m).

X-ray Scattering. X-ray scattering was performed on a Multiangle X-ray Scattering (MAXS) system using a Nonius FR591 rotating-anode generator operated at 40 kV and 85 mA.[26,27] A bright, highly collimated beam was obtained via Osmic Max-Flux optics and triple pinhole collimation under vacuum. Samples were loaded into 1.0 mm diameter glass capillaries (Charles Supper Co. Special Glass 10-SG), which were then flame-sealed. The scattering data were collected for 30 min using a Bruker Hi-Star multiwire two-dimensional detector at a sample-to-detector distance of 11 cm. The sample temperature was raised and maintained by a Linkam oven controlled via a Linkam TMS 94 temperature controller. The samples were heated to 120 °C and allowed to reach thermal equilibrium for 5 min prior to data collection. Two-dimensional data reduction and analysis of data were performed using the Datasqueeze software.[34]

Dielectric Relaxation Spectroscopy (DRS). Dielectric spectroscopy measurements were conducted on samples with thicknesses of 0.1 – 0.2 mm that were sandwiched between freshly polished brass electrodes with a top electrode diameter of 10 mm to form a parallel

plate capacitor cell. The sample / electrode sandwiches were positioned in a Novocontrol GmbH Concept 40 broadband dielectric spectrometer. The dielectric permittivity was measured using a sinusoidal voltage with amplitude 0.1 V over a 10^{-2} – 10^{7} Hz frequency range in all experiments. Data were collected in isothermal frequency sweeps every 5 K, from -50 to 150 °C.

3. Results and Discussion

A. ATR-FTIR. FTIR spectroscopy was used to augment earlier NMR characterization of the chemical structure of **ImBr** ionomers[33], as well as to provide insight on local ionic interactions and the nature of ethylene spacer ordering in the semi-crystalline ionomers. The important spectral regions of the four ionomers are displayed in Figure 2 with absorbance bands of particular interest highlighted. Above 2800 cm^{-1}, two intense absorbances are observed at ~2923 and 2850 cm^{-1}, which have been attributed to the alkyl C-H stretching modes of 1-methylimidazolium cations.[35,36] The imidazolium cation can further be identified by spectral features in the 1600 – 700 cm^{-1} region. The bands at ~ 1570 and 1460 cm^{-1} are indicative of imidazole ring stretching, the peak at 1165 cm^{-1} has been assigned to imidazole H–C–C and H–C–N bending, and the broad band centered near 750 cm^{-1} is attributed to the out of plane C–H bending mode of the imidazole ring.[37-39]

The formation of hydrogen bonds between the aromatic protons and the Br anion is evidenced by the presence of a peak between 3050 and 3080 cm^{-1}. Upon formation of C-H•••Br hydrogen bonds, the C-H bond stretching located at ~3130 cm^{-1} is weakened and its vibration frequency decreases.[36] As expected, the peak at 3050-3080 cm^{-1}, related to the

hydrogen bonds, and that at ~3130 cm^{-1}, attributed to the aromatic C-H not involved in hydrogen bonding, are relatively more intense for the ionomers containing a larger fraction of **ImBr** groups (**p9ImBr**). As the number of **ImBr** units decreases, the intensity of these peaks is also reduced **(p15ImBr, p21ImBr** and **r21ImBr)**.

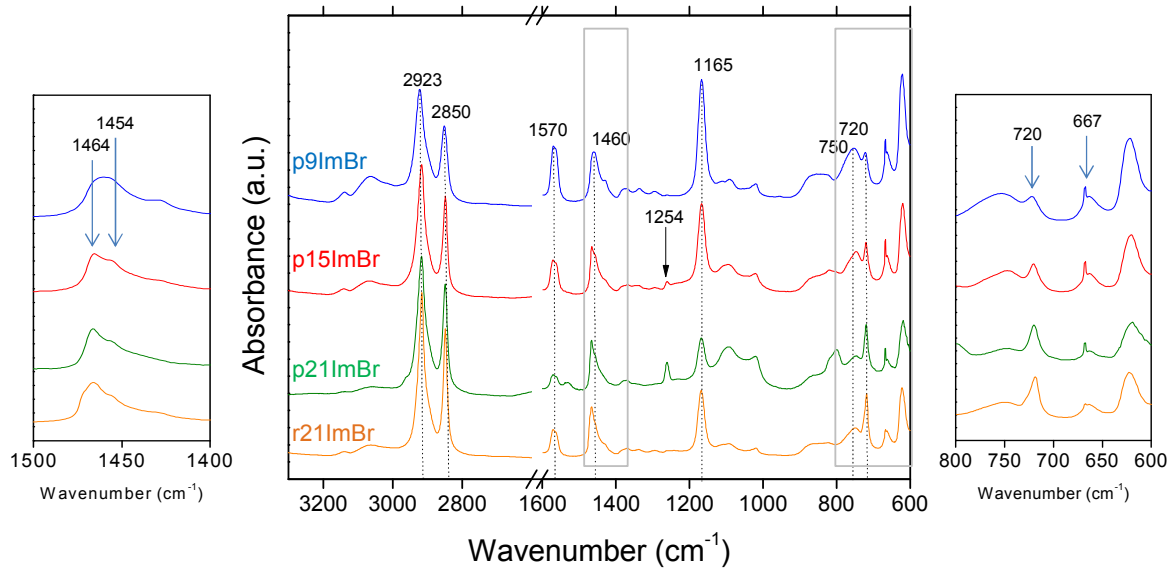

Figure 2. ATR-FTIR absorbance spectra of **ImBr** ionomers (**p9ImBr**, **p15ImBr**, **p21ImBr** and **r21ImBr**) in the region from 600 to 3300 cm^{-1} at room temperature. Data were shifted vertically for clarity. Scale expansion of the highlighted areas in the middle panel is provided in the left and right panels.

Another important spectral feature is the peak appearing at 720 cm^{-1}, corresponding to the CH_2 rocking vibrations, arising from both crystalline and amorphous segments of the PE spacers.[20,40-42] The relative absorbance at 720 cm^{-1} with respect to the imidazolium ring mode at 750 cm^{-1} increases with the PE segment length between precisely-placed **ImBr**

functionality. The CH_2 rocking vibration peak at 720 cm^{-1}, together with the band at 1462 cm^{-1} in the CH_2 bending region, can provide information on the crystalline unit cell. Based on previous results obtained by NMR and X-ray techniques on the same family of precise copolymers we would expect an orthorhombic crystalline phase.[27] Ethylene sequences in the typical orthorhombic PE unit cell display a doublet in the low frequency region that arises from long *trans* CH_2 sequences rocking at ~720 cm^{-1} and sequences of 5 or more CH_2 rocking at 730 cm^{-1}.[43] The absence of splitting in the CH_2 rocking mode (see Figure 2 - right panel), also not observed for other precise polyethylene-based copolymers,[20] may indicate some distortion of the orthorhombic unit cell in crystalline **ImBr** ionomers. In addition, Sworen, et al.[42] studied the evolution of the orthorhombic crystal of PE for random ethylene/propylene copolymers (characterized by a doublet at 719 and 730 cm^{-1} and single band at 1471 cm^{-1}) into a hexagonal unit cell, indicated by the appearance of methylene rocking (at 721 cm^{-1}) and scissoring (1466 cm^{-1}) modes. In the right panel of Figure 2 a single absorbance is observed at 720 cm^{-1}. At frequencies of ~1460 cm^{-1}, in addition to a contribution from the imidazolium rings, CH_2 scissoring is evidenced for the semi-crystalline samples, **p15ImBr**, **p21ImBr** and **r21ImBr** (Figure 2 - left panel). In summary we conclude that for semi-crystalline **ImBr** ionomers, the presence of crystals having a hexagonal unit cell, together with the orthorhombic crystals, cannot be excluded.

Additional information on ordered ethylene sequences can be obtained from the region between 1350 and 1250 cm^{-1}. The absence of crystallinity in **p9ImBr** (see also DSC results in section 3B) is evidenced by the presence of bands in the region between 1330 and 1353 cm^{-1},[41] which are weaker in the semi-crystalline samples. These

absorbances are related to the conformationally disordered ethylene sequences. A small peak is observed at 1254 cm^{-1} in **p15ImBr** and **p21ImBr** spectra, originating from conformationally ordered sequences, all-*trans*, composing the crystals. There is no detectable absorbance at 1254 cm^{-1} in the spectrum of the random ionomer **r21ImBr**, consistent with the proposal that precisely placed ionic groups favor order in the crystalline unit cells.[27]

FTIR spectroscopy also provides some insight on local conformations close to the **ImBr** pendant groups. The band at 622 cm^{-1} (Figure 2 - right panel) corresponds to the stretching of C−C side groups with vicinal C−C backbone carbons in an all-*trans* conformation, while the absorbance at 665 cm^{-1} corresponds to C−C stretching when the side group is adjacent to backbone carbons having *gauche* conformations.[35] The very narrow peak arising in the gauche conformation region for the precise ionomers may arise from rather ordered conformations at the **ImBr** aggregate interfaces, not evidenced in the spectrum of the random sample.

B. Thermal Analysis. Figure 3 displays the DSC thermograms of the precise[27] and random **ImBr** copolymers. Table 1 summarizes the glass transition temperatures (T_g), as well as melting temperatures (T_m) and enthalpies (ΔH_m) of the crystalline components in the ionomers. For **p9ImBr** the relatively large fraction of ionic pendants completely disrupts crystallization of the ethylene sequences, and this ionomer exhibits a single T_g with a midpoint of 15 ˚C. Clearly, aggregation of the ionic species (described in detail in

section 3C) has a rather strong effect on the T_g of the matrix segments, whose motion is slowed significantly via their attachment to the ionic domains.

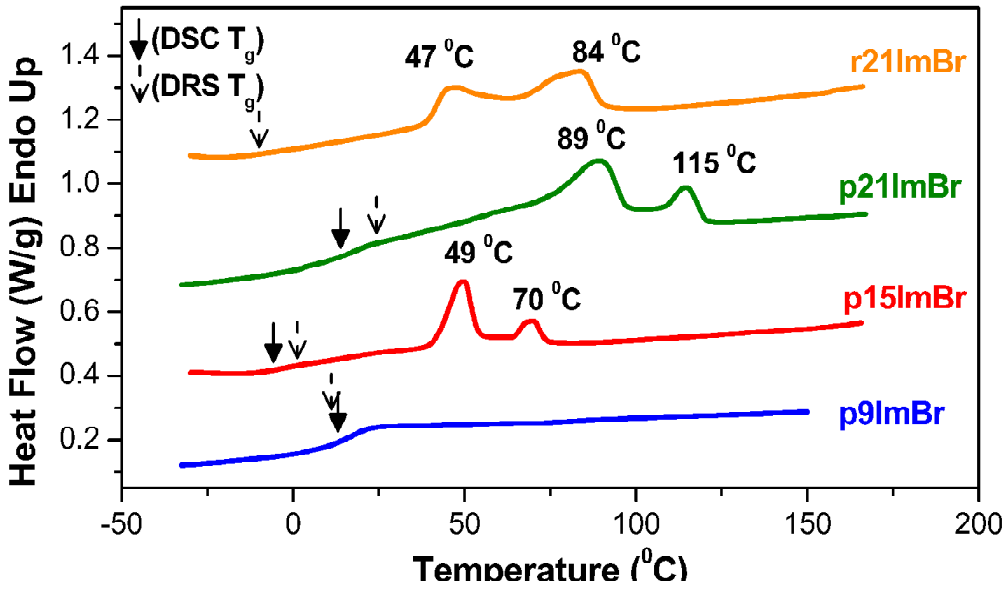

Figure 3. DSC thermal analysis of the precise[27] and pseudorandom ionomers. The solid arrows indicate the DSC T_gs for **p9ImBr**, **p15ImBr** and **p21ImBr**. The dashed arrows represent the $T_g s$ derived from dielectric spectroscopy by extrapolating the VFT fit of the segmental relaxation time to $\tau_\alpha (=1/\omega_\alpha) = 100$ s (referred to as DRS T_g). For clarity, the thermograms have been shifted vertically.

The T_g s for the semi-crystalline ionomers are more difficult to detect by DSC, although their segmental relaxations (dynamic glass transition) are clearly evident in dielectric loss spectra (section 3D). For the semi-crystalline precise ionomers (**p15ImBr**, **p21ImBr**), we detect relatively broad T_g s from DSC, but T_g is absent in the DSC data from **r21ImBr**. The amorphous phase dynamics will be discussed in detail in section 3D.

Table 1. Melting Points (T_m), Heats of Fusion (ΔH_m), Degrees of Crystallinity (X_c), Glass Transition Temperatures (T_g), Total Ion Concentration (p_0) and Refractive Indices (n) of the Precise and Pseudorandom **ImBr** Ionomers

	DSC				DRS		
	T_m (°C)	ΔH_m [a] (J/g)	X_c [b] (%)	$T_g \pm 3$ (°C)	$T_g \pm 10$ (°C)	p_0 [c] (nm^{-3})	n [c]
p9ImBr	-	-	-	15	13	2.73	1.64
p15ImBr	49 & 70	15	6	-5	1	2.14	1.69
p21ImBr	89 & 115	26	9	13	25	1.75	1.72
r21ImBr	47 & 84	30	11	-	-9	1.75	1.72

a) ΔH_m is the total enthalpy of the melting endotherms.

b) $X_c = \Delta H_m / \Delta H_m^{PE}$ ($\Delta H_m^{PE} = 277$ J/g, the perfect crystal heat of fusion for orthorhombic PE).[44]

c) Total ion concentration p_0 and n were determined based on the molecular structure.

Note that although **p15ImBr**, **p21ImBr**, and **r21ImBr** display clear melting endotherms (Figure 3), the degree of crystallinity under the crystallization conditions imposed here (Table 1) is very small compared to linear PE (~70-80%), on the order of 10% or lower, and their T_ms (Table 1) are well below that reported for linear PE synthesized by ADMET polymerization (133 °C).[21] The presence of the polar **ImBr** side groups, even when

precisely spaced, disrupts the ability of these materials to crystallize and slows crystallization considerably. As expected, ionomers with longer ethylene spacer lengths (decreasing ion content) lead to slightly higher degrees of crystallinity (X_c) and melting temperatures. Alamo, *et al.* have also observed an increase in T_m and X_c of PE with precision Cl placement as Cl content decreases.[21] In studies of other precise ethylene acid copolymers and ionomers, substitution of functional species (including acrylic acid and phosphonic acid with the mono or geminal substitution) on every 15th carbon atom has been found to completely suppress crystallization, in contrast to **p15ImBr**.[20,25-27] It has been proposed previously that the enhanced ordering of **p15ImBr** may arise from the relatively flexible CH_2 linkages between the ethylene backbone and ionic liquid pendant groups, as well as multiple hydrogen bonding sites in ionic liquids containing imidazolium bromide that facilitate ordering of the ionic species into sheet-like structures.[27,36] In contrast, the acrylic acid and phosphonic acid groups are attached directly to the polymer backbone.

As noted earlier, the precise and pseudorandom **ImBr** ionomers were rapidly cooled from the melt to room temperature then aged for at least 3 days. As a consequence of the slow crystallization kinetics of these materials due to the limited mobility imposed by the strongly interacting ionic pendant groups,[22,27,33] only a portion of the crystallinity of these materials is developed on cooling from the melt (i.e., at comparatively low degrees of supercooling) and this fraction is assigned to the higher temperature melting endotherms. As their T_gs are below room temperature, limited crystallization continues on aging (larger degrees of supercooling), and this portion of the crystallinity is assigned to the lower

temperature endotherms. Finally, the precise **p21ImBr** exhibits higher temperature melting endotherms compared to the compositionally identical pseudorandom analog **r21ImBr** (although both have a similar degrees of crystallinity). This arises from enhanced ordering in **p21ImBr** due to the precise regularity of the substitution.

C. X-ray Scattering. Figure 4a compares the room temperature X-ray scattering profiles for the four **ImBr** ionomers with different PE segment lengths and **ImBr** placement (precise vs pseudorandom). The amorphous **p9ImBr** exhibits two broad scattering peaks: the higher angle peak at scattering wavevector $q \approx 15\text{nm}^{-1}$ corresponds to the amorphous halo and the low-angle peak at $q \approx 3.5\text{nm}^{-1}$ is associated with the mean interaggregate scattering arising from the segregation of ionic groups.[27] The semi-crystalline ionomers, **p15ImBr**, **p21ImBr**, and **r21ImBr**, exhibit a sharp X-ray scattering peak near $q \approx 15\text{nm}^{-1}$, corresponding to the (110) reflection for orthorhombic PE at $q \approx 15.3\ \text{nm}^{-1}$.[27] This confirms the semi-crystalline nature of the PE matrix observed in FTIR (Figure 2) and DSC (Figure 3) measurements. **p15ImBr** and **p21ImBr** exhibit multiple scattering peaks (indicated by arrows in Figure 4a) at low angles that have positional ratios indicative of a layered morphology, indicating long-range order of the microphase-separated ion-containing layered aggregates.[27] The pseudorandom ionomer, **r21ImBr**, has a weak second peak that is consistent with a poorly-defined layered morphology. For the precise ionomers, the lowest-angle peak near $q \approx 3.5\text{nm}^{-1}$ shifts to lower q as the separation between **ImBr** functional groups in the chains increases, indicating as expected an increase in the average aggregate separation.[27]

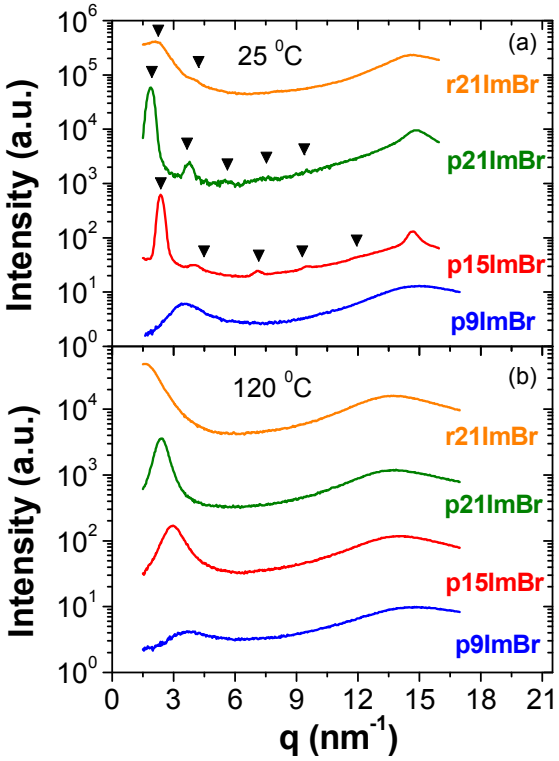

Figure 4. X-ray scattering intensity as a function of scattering wavevector q for the three precise and the pseudorandom ionomers at (a) 25 °C and (b) 120 °C.[26,27]

From earlier X-ray scattering studies[26,27] on precise ionomers, two morphologies have been identified based on the nature of the ionic aggregate resulting from microphase-separation of the ionic pendant groups and the PE matrix. When the PE segment is short (i.e., for **p9ImBr**) the material is amorphous and the ion pendants form aggregates that arrange with liquid-like order. When the PE segment length is longer (i.e., for **p15ImBr** and **p21ImBr**) and crystallizes, the precise ionomers exhibit layered morphologies at room temperature that contain ionic pendants arranged in sheets perpendicular to the PE spacers.

At 120 °C (see Figure 4b), above the T_m of the semi-crystalline materials, all ionomers exhibit liquid-like morphologies and the scattering maximum at low angle becomes broader and the higher order peaks are lost. Also at 120 °C the narrower, low-angle peak for **p21ImBr** broadens noticeably for the compositionally identical **r21ImBr** and is indicative of a more uniform distribution of interaggregate spacings in precise materials.[25]

D. Dielectric Relaxation

The segregated nature of ionic liquid pendant groups of the precise **ImBr** ionomers, as well as the crystallinity present for many of the materials, adds a degree of complexity to interpretation of the dielectric spectra. Although the **ImBr** ionomers do not exhibit high ionic conductivity per se (as shown later), conduction losses from ion motion are appreciable and can obscure loss peaks of interest, particularly at higher temperatures. Consequently, we use the derivative representation (ε_{der}),[45] which eliminates the conductivity contribution from dielectric loss spectra, to elucidate relaxation processes:[46-49]

$$\varepsilon_{der} = -\frac{\pi}{2}\frac{\partial \varepsilon'(\omega)}{\partial \ln \omega}. \quad (1)$$

where ω is the angular frequency. This method has been utilized to analyze dielectric loss spectra of other ion-containing polymers with notable success.[45-51] A representative example of the dielectric constant and loss along with ε_{der} are displayed as a function of frequency in Figure 5 for **p15ImBr** at 80 °C. The real part of the conductivity (σ') is also displayed in this plot and illustrates the usual definition of the dc conductivity (σ_{DC}) from conductivity spectra.

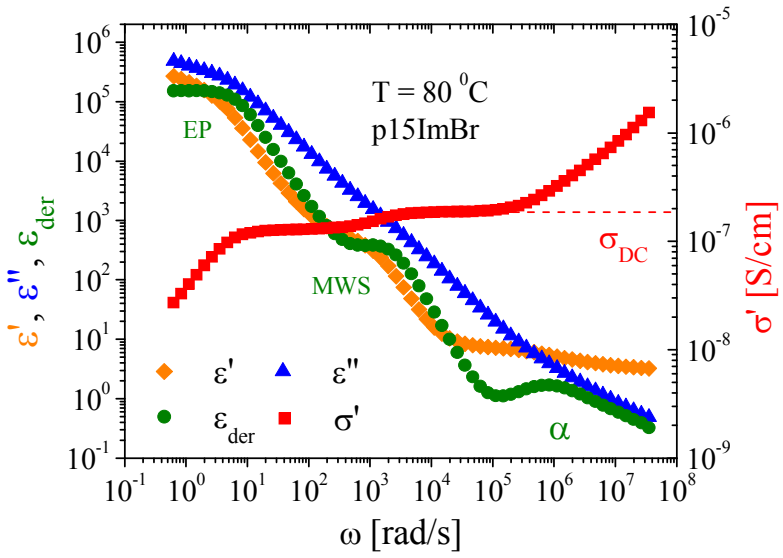

Figure 5. Representative isothermal plot of the dielectric constant (ε'), the dielectric loss (ε''), the derivative spectra (ε_{der}) and the real part of the conductivity (σ') for **p15ImBr** at 80 ˚C. σ_{DC} is indicated by the dotted red line.

Figure 6 displays a representative example of the derivative dielectric loss spectrum as a function of frequency and temperature for **p15ImBr**. Spectra of all **ImBr** precise ionomers exhibit a single segmental α relaxation at lower temperatures and two slower but very strong processes at higher temperatures. The interpretation of the faster process as a segmental relaxation is supported by its VFT character, and the strength (~10^2 – 10^4) of the intermediate temperature – lower frequency process is much too large to be associated with dipole relaxation (even ion dipoles) and is clearly associated with Maxwell-Wagner-Sillars (MWS) interfacial polarization. Since electrode polarization (EP, the highest temperature process), a phenomenon where transporting ions accumulate at the blocking electrodes,[52] is not a characteristic relaxation of the materials, we focus our

discussion primarily on the segmental α relaxations and include some discussion of the MWS processes.

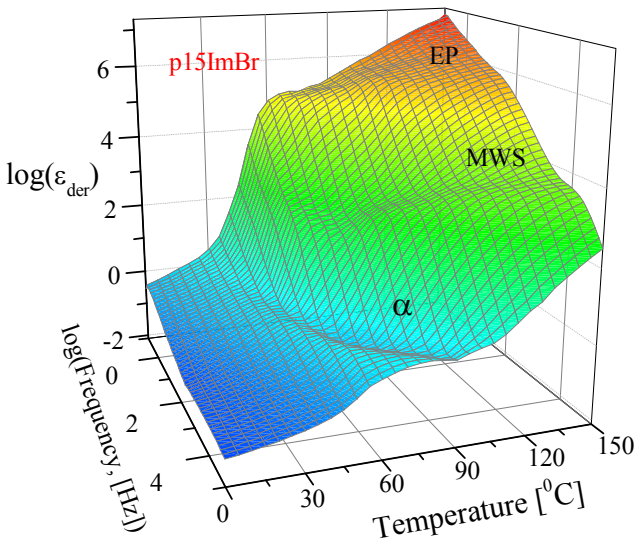

Figure 6. Representative conductivity-free dielectric derivative spectra ε_{der} as a function of frequency and temperature for **p15ImBr**.

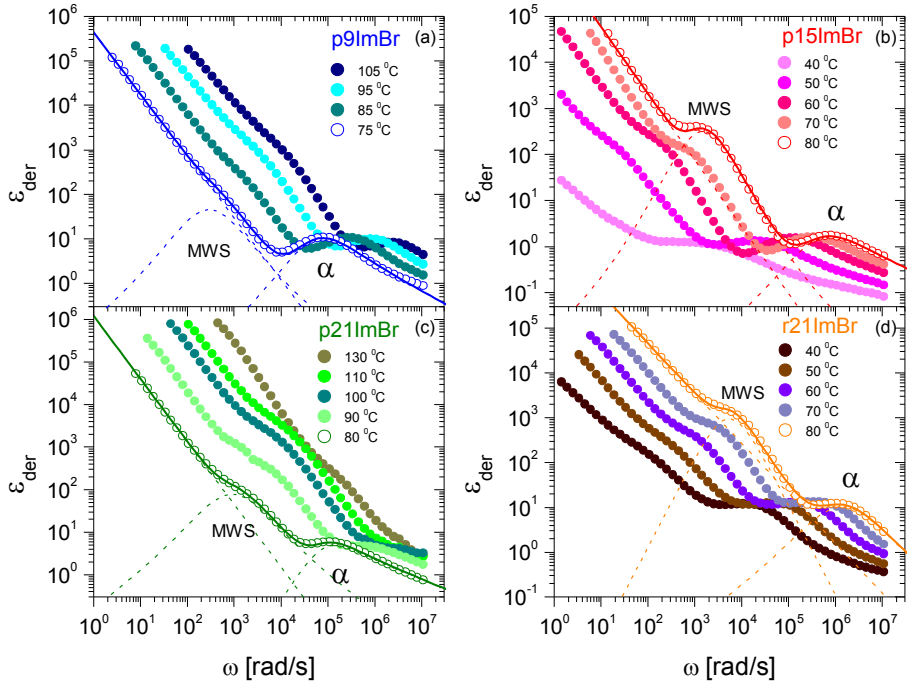

Figure 7. Derivative spectra ε_{der} of (a) **p9ImBr**, (b) **p15ImBr**, (c) **p21ImBr**, and (d) **r21ImBr** at selected temperatures. Solid lines (overlaying open symbols for one temperature in each panel) are fits to Eq. 2 with values of the EP power law slope (s) and shape parameters (a and b) of the two HN functions for MWS interfacial polarization and polymer segmental motion (α) for (a) **p9ImBr**: $s = 1.27 \pm 0.17$, $a_{MWS} = 1$, $b_{MWS} = 1$, $a_\alpha = 0.83 \pm 0.10$, and $b_\alpha = 0.77 \pm 0.17$ and for (b) **p15ImBr**: $s = 1.36 \pm 0.12$, $a_{MWS} = 1$, $b_{MWS} = 1$, $a_\alpha = 0.82 \pm 0.18$, and $b_\alpha = 0.55 \pm 0.14$ and for (c) **p21ImBr**: $s = 1.51 \pm 0.17$, $a_{MWS} = 0.87 \pm 0.07$, $b_{MWS} = 1$, $a_\alpha = 0.90 \pm 0.08$, and $b_\alpha = 0.51 \pm 0.10$ and for (d) **r21ImBr**: $s = 1.15 \pm 0.15$, $a_{MWS} = 0.81 \pm 0.11$, $b_{MWS} = 1$, $a_\alpha = 0.81 \pm 0.09$, and $b_\alpha = 1$. For the same selected temperatures in each panel, individual contributions of the relaxations are shown as dashed lines.

The derivative spectra were then fit using a sum of a power law[53] for EP and two separate derivative forms of the Havriliak-Negami (HN) function for the MWS and α relaxation peaks (Figure 7):

$$\varepsilon_{\text{der}} = A\omega^{-s} - \frac{\pi}{2}\left(\left[\frac{\partial\varepsilon'_{\text{HN}}(\omega)}{\partial\ln\omega}\right]_{\text{MWS}} + \left[\frac{\partial\varepsilon'_{\text{HN}}(\omega)}{\partial\ln\omega}\right]_{\alpha}\right) \text{ with } \varepsilon'_{\text{HN}}(\omega) = \text{Real}\left\{\frac{\Delta\varepsilon}{\left[1+(i\omega/\omega_{\text{HN}})^{a}\right]^{b}}\right\}, \quad (2)$$

where A and s are constants, $\Delta\varepsilon$ is the relaxation strength, a and b are the shape parameters[54] and ω_{HN} is a characteristic frequency related to the frequency of maximum loss ω_{max} by:

$$\omega_{\text{max}} = \omega_{\text{HN}}\left(\sin\frac{a\pi}{2+2b}\right)^{1/a}\left(\sin\frac{ab\pi}{2+2b}\right)^{-1/a}. \quad (3)$$

The peak relaxation frequency ω_{max} and relaxation strength $\Delta\varepsilon$ of the MWS and α processes are determined from this fitting. On heating, the strength of the MWS process generally increases with temperature (along with σ_{DC}), and eventually merges with electrode polarization.

Segmental α process. The α process involves segmental motion of the polymer and hence exhibits typical characteristics of the glass transition dynamics. Representative behavior of the α relaxation as a function of temperature and frequency is displayed in Figure 8 for **p9ImBr**. It is important to point out that although the ionic liquid pendant groups are generally aggregated in this family of precise and pseudo-random ethylene ionomers, some fraction of the **ImBr** species clearly participates in the α relaxation as determined from experimental relaxation strengths (Figure 9b). This indicates that not all

of the **ImBr** species are fully immobilized in aggregates when using the processing conditions employed in the present study, and/or that aggregates are not symmetric and have a net dipole moment.

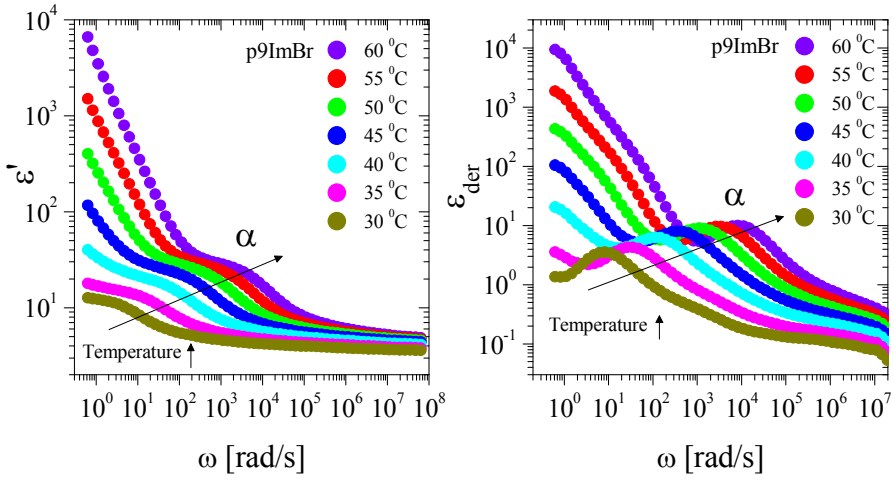

Figure 8. The dielectric constant (left) and derivative spectra (right) of **p9ImBr** as a function of temperature in the region of the dielectric spectrum where the α process is clearly observed.

The α peak relaxation frequencies are fit to the Vogel-Fulcher-Tammann (VFT) equation (see Figure 9a),

$$\omega_{\max} = \omega_{\infty} \exp\left(-\frac{DT_0}{T - T_0}\right), \tag{4}$$

where ω_{∞} is the high-temperature limiting frequency, D is the so-called strength parameter, and T_0 is the Vogel temperature, listed in Table 2. The T_gs determined from DSC and those

determined from the segmental relaxation by extrapolating the VFT fit of the peak relaxation time to $\tau_\alpha(=1/\omega_\alpha)=100$ s [55] are in relatively good agreement within experimental uncertainty (see Table 1). Note that the T_gs from DRS are determined by extrapolation from the amorphous state. As noted earlier, although a DSC T_g could not be detected for **r21ImBr**, presumably arising from increased breadth and relatively small heat capacity change at T_g, the α relaxation is clearly visible in dielectric loss spectra.

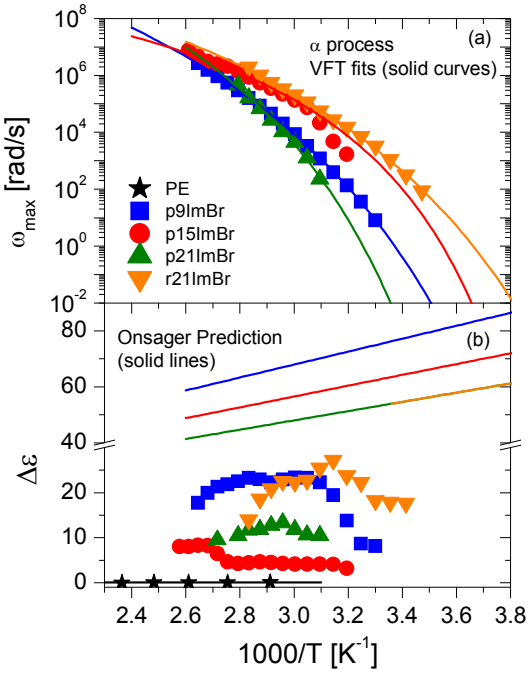

Figure 9. (a) Temperature dependence of relaxation frequency maxima ω_{max} of the α process: solid curves are fits of the VFT equation (Eq. 4).[56] (b) Temperature dependence of relaxation strength $\Delta\varepsilon$ of the α process: solid lines are predictions of the Onsager equation (with fixed concentration and strength of dipoles and assuming the Kirkwood correlation factor $g=1$).

Table 2. Fitting Parameters (Eq. 4) of the VFT Temperature Dependence and Fragility m of the α Process.

	$\log(\omega_\infty)$ (rad/s)	D	T_0 (˚C)	DRS T_g (˚C)	DRS $T_g - T_0$ (˚C)	(DRS $T_g - T_0$)/D (˚C)	$m^a \pm 10$
p9ImBr	13.2	12.5	-63	13	76	6.0	57
p15ImBr	10.1	5.0	-41	1	42	8.4	79
p21ImBr	13.5	9.5	-38	25	63	6.6	73
r21ImBr	11.0	7.7	-63	-9	54	7.0	63

a) m determined from Eq. 5 using the VFT fit parameters for the segmental (α) peak frequency (Figure 9a).

As seen Table 1, the T_gs determined for the precise **ImBr** ionomers vary over a modest temperature range when changing composition (and in the same fashion in DSC and DRS experiments). However, these (and correspondingly the ω_{max} in Figure 9a) vary in a non-systematic fashion, depending on composition, crystallinity and morphology. Using the relaxation of amorphous **p9ImBr** as a 'baseline', the α process becomes somewhat faster for **p15ImBr**, which contains longer ethylene spacer lengths between **ImBr** pendant groups. The α process then slows down for **p21ImBr**, becoming comparable to amorphous **p9ImBr**, presumably due to the influence of additional ethylene crystallization on the segmental dynamics. Even though **p21ImBr** and **r21ImBr** are compositionally identical and exhibit similar crystallinities, the α relaxation for the polymer with random **ImBr** placement is considerably faster than that of **p21ImBr**. This is

a clear manifestation of the important role of precise vs random pendant group placement on polymer dynamics, and likely arises from the occasional longer than average ethylene sequences in **r21ImBr** and perhaps also from the poorly-defined layered morphology of **r21ImBr**.

The parameter D in Eq. 4 is related to the fragility (i.e., deviation from Arrhenius behavior), providing additional information about the segmental relaxation time in the vicinity of T_g. The fragility m can be determined from:[57]

$$m = -\left.\frac{d\log(\omega)}{d(T_g/T)}\right|_{T=T_g} = \frac{DT_0}{T_g(\ln 10)(1-T_0/T_g)^2}, \quad (5)$$

wherein D and T_0 are VFT fitting parameters for ω_α (Figure 9a), using $T_g = \text{DRS } T_g$. The estimated fragility m values of the semi-crystalline **p15ImBr** and **p21ImBr** ionomers (Table 2) are essentially the same, while those for amorphous **p9ImBr** and crystalline **r21ImBr** appear at first glance to be slightly lower ($m \sim 60$). However, due to the limited number of data points available for this analysis (due to overlap of the segmental relaxation with MWS polarization) the uncertainty in the m values in Table 2 is approximately ± 10, and consequently all are the same within experimental uncertainty. Prior observations have demonstrated the invariance of fragility with the presence and degree of crystallinity in other semi-crystalline polymers.[58-60]

Figure 9b displays the temperature dependence of the experimental relaxation strengths $\Delta\varepsilon$ of the α process for these ionomers and non-ionic polyethylene (PE). All ionomers clearly have much higher $\Delta\varepsilon_\alpha$ than the non-ionic PE.[61] The increase in the strength arises from the enhanced dipole moment imparted by the ionic groups composed

of imidazolium cations and Br^- anions. Given the disparity in chemical nature of the PE matrix and ionic liquid pendants as well as the sharp maxima observed in X-ray scattering, we adopt the view that all **ImBr** units reside in ionic aggregates. Consequently, this signifies that not all of the **ImBr** species are fully immobilized in aggregates and/or that aggregates are not symmetric and exhibit a net dipole moment.

As expected at higher temperatures, $\Delta\varepsilon_\alpha$ generally decreases with increasing temperature due to thermal dipole randomization. However, for the ionomers where $\Delta\varepsilon_\alpha$ can be reliably determined over a wider temperature range (**p9ImBr** and **r21ImBr**) the relaxation strength at lower temperatures is observed to increase significantly with temperature, indicating greater participation of ion dipoles in the segmental relaxation as temperature is increased.

We first consider the temperature dependence of $\Delta\varepsilon$ for these ionomers by utilizing the Onsager relationship,[47,48,62]

$$\frac{\Delta\varepsilon(2\Delta\varepsilon+3\varepsilon_\infty)}{(\Delta\varepsilon+\varepsilon_\infty)(\varepsilon_\infty+2)^2}=\frac{1}{9\varepsilon_0 kT}\sum_i \nu_i m_i^2, \quad (6)$$

where ν_i is the number density of dipoles, m_i is their dipole moment, k is the Boltzmann constant, T is absolute temperature, and ε_∞ is the high-frequency limit of the dielectric constant (here taken to as $\varepsilon_\infty = n^2$, where n is the refractive index, estimated from group contributions[63] and listed in Table 1). The black solid line in Figure 9b is the fit to Eq. 6 with the $\sum_i \nu_i m_i^2$ term as the sole fitting parameter, showing that $\Delta\varepsilon$ of the non-ionic PE is well described by the Onsager equation. For the ionomers with imidazolium cation - Br

anion pendant groups, the contribution of the ions to the relaxation strength can be analyzed[47,48,64] by first considering the influence of contact ion pairs to Eq. 6:

$$\left[\frac{\Delta\varepsilon(2\Delta\varepsilon+3\varepsilon_\infty)}{(\Delta\varepsilon+\varepsilon_\infty)(\varepsilon_\infty+2)^2}\right]_{\text{ionomer}} = \frac{\nu_{\text{pair}} m_{\text{pair}}^2}{9\varepsilon_0 kT} + \left[\frac{\Delta\varepsilon(2\Delta\varepsilon+3\varepsilon_\infty)}{(\Delta\varepsilon+\varepsilon_\infty)(\varepsilon_\infty+2)^2}\right]_{\text{nonionic}}, \quad (7)$$

where ν_{pair} is the number density of ion pairs and m_{pair} is their dipole moment. For the dielectric constant range ($\varepsilon \sim 15 \pm 10$) of these ionomers, all ions are expected to remain paired because the coulombic interactions between anions and cations are strong (Bjerrum length [$1\text{ nm} < l_B \equiv e^2/(4\pi\varepsilon\varepsilon_0 kT) < 11\text{ nm}$], suggesting a pair energy > 60 ± 30 kT). The solid lines in Figure 9b are the Onsager predictions of Eq. 7 for each ionomer, for the hypothetical case where all ions are in the isolated ion pair state ($\nu_{\text{pair}} = p_0$, listed in Table 1) with the contact pair dipole moment ($m_{\text{pair}} = 8.7$ D, determined from *ab initio* calculations[65]). Since **ImBr** groups are clearly seen in the X-ray scattering experiments to be aggregated and dynamic mechanical data reported in ref 33 displays a rubbery plateau consistent with aggregates reinforcing the polymer melt, it is expected and observed experimentally that the dielectric relaxation strengths for these ionomer are well below that of the corresponding Onsager prediction from Eq. 7. These ionomers are more polar than the non-ionic PE, but their ions are aggregated and largely immobilized at these temperatures, analogous to zinc-neutralized sulfonated polystyrene ionomers.[51] Nevertheless, the fact that the relaxation strength of the segmental process is much stronger than that of PE indicates that some fraction of **ImBr** pendants participates in the α process.

Since ionic species in aggregates are expected to lead to correlation of neighboring ion dipoles, one can estimate the fraction of the **ImBr** functional groups participating in

the α relaxation of the precise ionomers by determining the Kirkwood – Fröhlich g factor (i.e., the dipole correlation factor): [66,67,68]

$$g = \frac{9\varepsilon_0 kT}{\nu_{\text{pair}} m_{\text{pair}}^2} \left\{ \left[\frac{\Delta\varepsilon(2\Delta\varepsilon + 3\varepsilon_\infty)}{(\Delta\varepsilon + \varepsilon_\infty)(\varepsilon_\infty + 2)^2} \right]_{\text{ionomer}} - \left[\frac{\Delta\varepsilon(2\Delta\varepsilon + 3\varepsilon_\infty)}{(\Delta\varepsilon + \varepsilon_\infty)(\varepsilon_\infty + 2)^2} \right]_{\text{nonionic}} \right\}, \quad (8)$$

which is a measure of the effect of dipole interactions on the experimental relaxation strength. Dipole correlation factors were calculated from Eq. 8 for the case in which all ions are in the isolated ion pair state ($\nu_{\text{pair}} = p_0$ where p_0 is the total ion number density, listed in Table 1) with the contact pair dipole moment ($m_{\text{pair}} = 8.7$ D). For **p9ImBr**, $g \sim 0.2$ – 0.4, indicating that (depending on temperature) about 20 – 40% of the ion dipoles in this ionomer contribute to the α relaxation, with ~60-80% either immobilized or having net anti-parallel arrangement in ion aggregates. The g-factors for **p15ImBr** and **p21ImBr** are similar, ranging from 0.1 – 0.2 for **p15ImBr** and 0.2 – 0.3 for **p21ImBr**. However, as can be inferred from Figure 9b, considerably more **ImBr** ion dipoles participate in the α process for the compositionally identical but pseudo-random **r21ImBr** ($g \sim 0.4 - 0.6$ depending on temperature), compared to **p21ImBr**. This is again a clear indication of the important role of precise vs random pendant group placement on the polymer dynamics. The origin of this difference is connected with the irregular ethylene sequence lengths and the poorly-defined layered morphology in **r21ImBr**, leading to relatively fewer ions fully immobilized in aggregates or that the relatively poorly organized aggregates in **r21ImBr** exhibit a comparatively larger net dipole moment than those in the precise ionomers. Finally, it is worth noting that in our recent study of precise ethylene – acrylic acid copolymers with carboxylic acid functionality on every 9th, 15th or 21st carbon,[69] FTIR

spectroscopy demonstrates that all of the acid groups exist in hydrogen-bonded dimers (and these assemble into acid aggregates). The dielectric relaxation strengths of the α processes for the precise acrylic acid – containing materials are comparatively very small, suggesting that the smaller acid functionality is more tightly bound in aggregates compared with the larger **ImBr** groups in the precise copolymers described herein.

Interfacial Polarization. Differences in dielectric permittivity and conductivity of the phases in heterogeneous materials give rise to interfacial polarization due to accumulation of charges near the interfaces between the various phases.[52] Such polarization typically occurs at frequencies lower than that of matrix segmental relaxation (and the onset of ion motion in the matrix phase) and with high relaxation strength. This interfacial polarization is referred to Maxwell-Wagner-Sillars polarization and has been studied previously for emulsions, multi-phase blends, block copolymers, and semi-crystalline polymers.[52,70] Since all of the **ImBr** ionomers are clearly microphase-separated from the X-ray scattering measurements up to at least 120 ˚C (Figure 4), we expect the relaxation process observed at lower frequency in Figure 7 to originate from charge build-up at the interfacial boundary between the microphase-separated aggregates (ion domains and lamellar interfaces) in a predominately non-polar PE matrix. As noted earlier, the observed relaxation strength of this process is on the order of $10^2 – 10^4$, which is far too large to be attributed to dipolar motions.

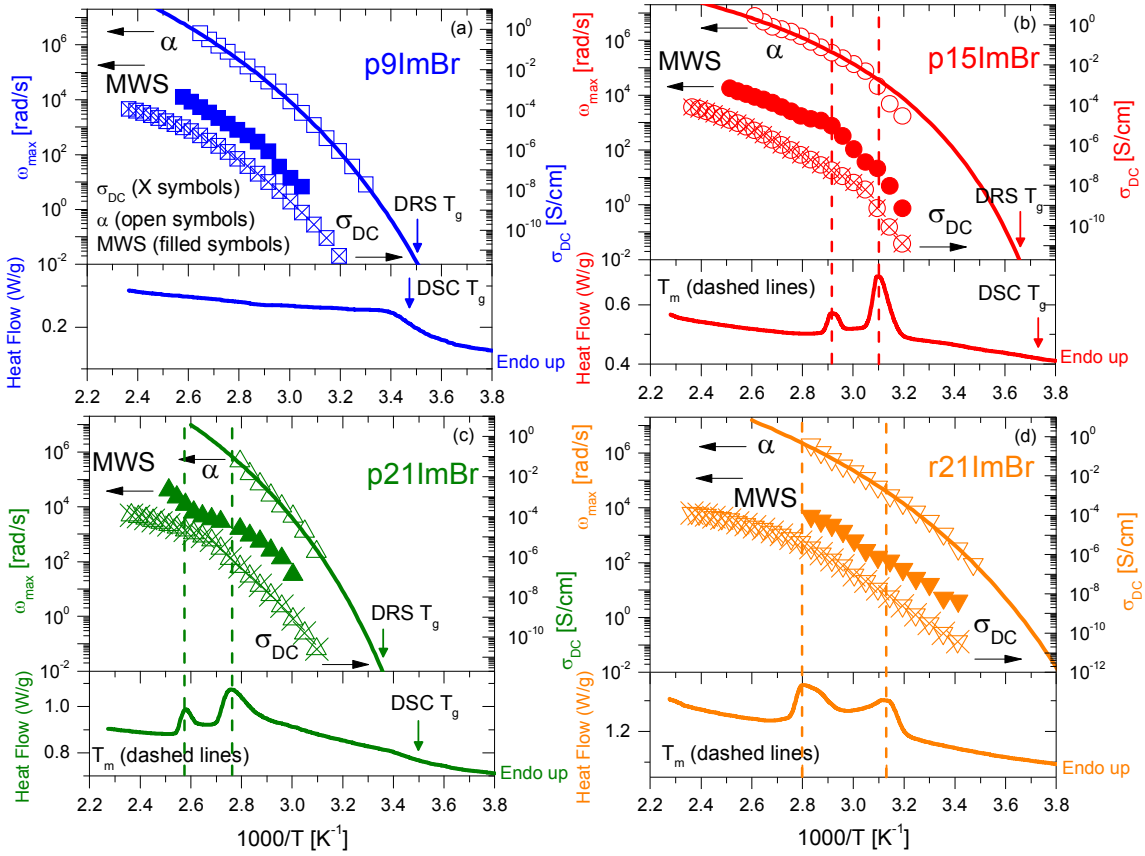

Figure 10. Temperature dependence of relaxation frequency ω_{max} for MWS process (filled symbols), α process (open symbols) and DC conductivity σ_{DC} (X symbols), along the DSC thermograms (solid lines) for (a) **p9ImBr**, (b) **p15ImBr**, (c) **p21ImBr**, and (d) **r21ImBr**. Vertical dashed lines indicate melting (T_m) transition temperatures from DSC and solid curves are VFT fits to the α relaxation frequencies.

The frequency and strength of the MWS process depend on the dielectric contrast (i.e., the difference in dielectric constant and conductivity) between the matrix and the microphase-separated ionic aggregates. Figure 10 shows that the relaxation frequencies for the interfacial MWS relaxation (ω_{MWS}, filled symbols) and DC conductivity (σ_{DC}, X

symbols), along with the DSC thermograms (plotted as 1/T, solid lines) for all four ionomers. Note that σ_{DC} is rather low (ca. 10^{-9} – 10^{-11} S/cm) for these materials at 40 ˚C, consistent with the segregated nature of the ionic species in the PE matrix and absence of significant ion domain connectivity. However, σ_{DC} increases rapidly as temperature increases well above T_g, generally following the expected VFT temperature dependence.

The peak relaxation frequencies of the MWS process follow a similar temperature dependence as their DC conductivity. Moreover, at the observed melting transitions (indicated by vertical dashed lines in Figure 10), the temperature dependence of ω_{MWS} and σ_{DC} exhibit a change in slope. This is additional evidence for the assignment of this process as originating from MWS polarization. Although not shown here, the relaxation strengths of the MWS process also depend strongly on temperature in the melting region. The MWS process does not disappear above T_m of the semi-crystalline **ImBr** ionomers, in agreement with findings from the higher temperature X-ray scattering experiments (Figure 4b) that ionic aggregates persist to high temperatures.

4. Summary

In this paper we report on the molecular dynamics of three polyethylene-based **ImBr** precise ionomers and one pseudorandom ionomer, in light of their microphase-separated morphologies. FTIR spectroscopy provides evidence of hydrogen bond formation between the aromatic protons and Br anions of **ImBr** pendants. X-ray scattering measurements demonstrate that semi-crystalline **p15ImBr, p21ImBr** and **r21ImBr** at room temperature exhibit layered morphologies, i.e., the ionic groups form planar aggregates that stack with

long-range order, whereas amorphous **p9ImBr** exhibits ionic aggregates with liquid-like packing. All four of the **ImBr** precise ionomers exhibit liquid-like ordering of the microphase-separated ion aggregates at 120 ˚C.

DSC experiments confirmed the presence of crystallinity in the precise or pseudorandom ionomers with longer ethylene spacer length between pendant **ImBr** groups (**p15ImBr**, **p21ImBr** and **r21ImBr**). The degree of crystallinity is quite low however (on the order of 10%) as are the T_ms: the presence of the relatively large and polar **ImBr**, even when precisely spaced, severely disrupts the ability of the polyethylene sequences to crystallize under the preparation conditions used herein.

All of the ionomers display a single DSC T_g (when one can be determined) and correspondingly a single α process in dielectric relaxation experiments. T_gs range from approximately -9 to 20 ˚C depending on **ImBr** composition, ethylene segment crystallinity and microphase-separated morphology, and reflect the considerable slowing down of the motion of the matrix segments due to their attachment to ionic domains. **r21ImBr,** although compositional identical and having a similar crystallinity, exhibits significantly faster α relaxation dynamics compared to **p21ImBr**. This is in keeping with the important role of precise vs random pendant group placement on polymer segmental dynamics, and likely arises from the occasional longer than average ethylene sequences in **r21ImBr**.

As the X-ray scattering experiments clearly demonstrate that **ImBr** groups are aggregated, it is expected and observed experimentally that the segmental relaxation strengths for these ionomers are well below that of the corresponding Onsager prediction. However, $\Delta\varepsilon_\alpha$ was found to be much larger than that of PE alone and indicates that some

fraction of **ImBr** pendants participates in the α process. Based on our proposal that all **ImBr** units reside in ionic aggregates, this suggests that not all of the **ImBr** species are fully immobilized in aggregates and/or that aggregates are not symmetric and exhibit a net dipole moment. Kirkwood dipole correlation factors were calculated for the precise **ImBr** ionomers to estimate the fraction of **ImBr** species participating in segmental relaxation. For the precise ionomers, calculated *g*-factors range from ca. 0.1 – 0.4, depending on polymer composition and temperature. In other words, ~10 – 40% of the ion dipoles participate in the segment process for the precise ionomers, with the remainder immobilized or with net anti-parallel orientation in aggregates. However, considerably more **ImBr** ion dipoles participate in the α process for the compositionally identical but pseudo-random **r21ImBr** ($g \sim 0.4 – 0.6$ depending on temperature), compared to **p21ImBr**. This is again a clear indication of the important role of precise vs random pendant group placement on the polymer segmental dynamics.

Acknowledgments. This work was supported by the National Science Foundation, Polymers Program, under awards DMR-1206571 (Runt) and DMR-1103858 (Winey). This material is also based upon work supported by the National Science Foundation under Grant No. DMR-1203136. Any opinions, findings, and conclusions or recommendations expressed are those of the authors and do not necessarily reflect the views of the U.S. National Science Foundation. We are grateful to Dr. Amalie L. Frischknecht and Dr. Mark J. Stevens (both at Sandia National Laboratories) for helpful discussions.

References

(1) Eisenber, A. *Adv. Polymer Sci.* **1967**, *55*, 59-112.

(2) Eisenber, A.; Kim, J. S. *Introduction to ionomers*; Wiley: New York, 1998.

(3) Grady, B. P. *Polym. Eng. Sci.* **2008**, *48*, 1029-1051.

(4) Tant, M. R.; Mauritz, K. A.; Wilkes, G. L. *Ionomers: synthesis, structure, properties and applications*; Blackie Academic & Professional: London, 1997.

(5) Armand, M.; Bruce, P. G.; Forscyth, M.; Scrosati, B.; Wieczorek, W. In *Energy materials*; Bruce, D. W., O'Hare, D., Walton, R. I., Eds.; Wiley: New York, 2011.

(6) Bouchet, R.; Maria, S.; Meziane, R.; Aboulaich, A.; Lienafa, L.; Bonnet, J.-P.; Phan, T. N. T.; Bertin, D.; Gigmes, D.; Devaux, D.; Denoyel, R.; Armand, M. *Nat. Mater.* **2013**, *12*, 452-457.

(7) *Ionomers: Characterization, Theory and Applications*; Schlick, S., Ed.; CRC Press: Boca Raton, 1996.

(8) Eisenberg, A.; Hird, B.; Moore, R. B. *Macromolecules* **1990**, *23*, 4098-4107.

(9) Laurer, J. H.; Winey, K. I. *Macromolecules* **1998**, *31*, 9106-9108.

(10) Kutsumizu, S.; Tagawa, H.; Muroga, Y.; Yano, S. *Macromolecules* **2000**, *33*, 3818-3827.

(11) Sauer, B. B.; McLean, R. S. *Macromolecules* **2000**, *33*, 7939-7949.

(12) Taubert, A.; Winey, K. I. *Macromolecules* **2002**, *35*, 7419-7426.

(13) Benetatos, N. M.; Winey, K. I. *J. Polym. Sci. Part B: Polym. Phys.* **2005**, *43*, 3549-3554.

(14) Loo, Y.-L.; Wakabayashi, K.; Huang, Y. E.; Register, R. A.; Hsiao, B. S. *Polymer*

2005, *46*, 5118-5124.

(15) Wakabayashi, K.; Register, R. A. *Polymer* **2005**, *46*, 8838-8845.

(16) Wakabayashi, K.; Register, R. A. *Macromolecules* **2006**, *39*, 1079-1086.

(17) Scogna, R. C.; Register, R. A. *J. Polym. Sci. Part B: Polym. Phys.* **2009**, *47*, 1588-1598.

(18) Scogna, R. C.; Register, R. A. *Polymer* **2009**, *50*, 585-590.

(19) Boz, E.; Wagener, K. B.; Ghosal, A.; Fu, R.; Alamo, R. G. *Macromolecules* **2006**, *39*, 4437-4447.

(20) Baughman, T. W.; Chan, C. D.; Winey, K. I.; Wagener, K. B. *Macromolecules* **2007**, *40*, 6564-6571.

(21) Alamo, R. G.; Jeon, K.; Smith, R. L.; Boz, E.; Wagener, K. B.; Bockstaller, M. R. *Macromolecules* **2008**, *41*, 7141-7151.

(22) Rojas, G.; Inci, B.; Wei, Y. Y.; Wagener, K. B. *J. Am. Chem. Soc.* **2009**, *131*, 17376-17386.

(23) Opper, K. L.; Markova, D.; Klapper, M.; Mullen, K.; Wagener, K. B. *Macromolecules* **2010**, *43*, 3690-3698.

(24) Hall, L. M.; Seitz, M. E.; Winey, K. I.; Opper, K. L.; Wagener, K. B.; Stevens, M. J.; Frischknecht, A. L. *J. Am. Chem. Soc.* **2012**, *134*, 574-587.

(25) Seitz, M. E.; Chan, C. D.; Opper, K. L.; Baughman, T. W.; Wagener, K. B.; Winey, K. I. *J. Am. Chem. Soc.* **2010**, *132*, 8165-8174.

(26) Buitrago, C. F.; Alam, T. M.; Opper, K. L.; Aitken, B. S.; Wagener, K. B.; Winey, K. I. *Macromolecules* **2013**, *46*, 8995-9002.

(27) Buitrago, C. F.; Jenkins, J. E.; Opper, K. L.; Aitken, B. S.; Wagener, K. B.; Alam, T. M.; Winey, K. I. *Macromolecules* **2013**, *46*, 9003-9012.

(28) Buitrago, C. F.; Opper, K. L.; Wagener, K. B.; Winey, K. I. *Acs Macro Lett.* **2012**, *1*, 71-74.

(29) Bolintineanu, D. S.; Stevens, M. J.; Frischknecht, A. L. *Acs Macro Lett.* **2013**, *2*, 206-210.

(30) Bolintineanu, D. S.; Stevens, M. J.; Frischknecht, A. L. *Macromolecules* **2013**, *46*, 5381-5392.

(31) Hall, L. M.; Stevens, M. J.; Frischknecht, A. L. *Phys. Rev. Lett.* **2011**, *106*, 127801.

(32) Lueth, C. A.; Bolintineanu, D. S.; Stevens, M. J.; Frischknecht, A. L. *J. Chem. Phys.* **2014**, *140*, 054902.

(33) Aitken, B. S.; Buitrago, C. F.; Heffley, J. D.; Lee, M.; Gibson, H. W.; Winey, K. I.; Wagener, K. B. *Macromolecules* **2012**, *45*, 681-687.

(34) Heiney, P. A. *Comm. Powder Diffr. Newsl.* **2005**, *32*, 9-11.

(35) Kaner, P.; Ruiz-Orta, C.; Boz, E.; Wagener, K. B.; Tasaki, M.; Tashiro, K.; Alamo, R. G. *Macromolecules* **2014**, *47*, 236-245.

(36) Elaiwi, A.; Hitchcock, P. B.; Seddon, K. R.; Srinivasan, N.; Tan, Y. M.; Welton, T.; Zora, J. A. *Dalton Trans.* **1995**, 3467-3472.

(37) Berg, R. W.; Deetlefs, M.; Seddon, K. R.; Shim, I.; Thompson, J. M. *J. Phys. Chem. B* **2005**, *109*, 19018-19025.

(38) Holomb, R.; Martinelli, A.; Albinsson, I.; Lassègues, J. C.; Johansson, P.; Jacobsson, P. *J. Raman Spectrosc.* **2008**, *39*, 793-805.

(39) Nath, A. K.; Kumar, A. *Ionics* **2013**, *19*, 1393-1403.

(40) HSU, T. S. *J. Polym. Sci. Pol. Phys.* **1980**, *18*, 2379-2389.

(41) Hagemann, H.; Strauss, H. L.; Snyder, R. G. *Macromolecules* **1987**, *20*, 2810-2819.

(42) Sworen, J. C.; Smith, J. A.; Wagener, K. B.; Baugh, L. S.; Rucker, S. P. *J. Am. Chem. Soc.* **2003**, *125*, 2228-2240.

(43) Snyder, R. G. *J. Mol. Spectrosc.* **1961**, *7*, 116-144.

(44) Brandrup, J.; Immergut, E. H. *Polymer Handbook*; John Wiley & Sons: New York, 1989.

(45) Wübbenhorst, M.; van Turnhout, J. *J. Non-Cryst. Solids* **2002**, *305*, 40-49.

(46) Fragiadakis, D.; Dou, S.; Colby, R. H.; Runt, J. *Macromolecules* **2008**, *41*, 5723-5728.

(47) Fragiadakis, D.; Dou, S.; Colby, R. H.; Runt, J. *J. Chem. Phys.* **2009**, *130*, 064907.

(48) Choi, U. H.; Lee, M.; Wang, S.; Liu, W.; Winey, K. I.; Gibson, H. W.; Colby, R. H. *Macromolecules* **2012**, *45*, 3974-3985.

(49) Choi, U. H.; Mittal, A.; Price, T. L.; Gibson, H. W.; Runt, J.; Colby, R. H. *Macromolecules* **2013**, *46*, 1175-1186.

(50) Castagna, A. M.; Wang, W.; Winey, K. I.; Runt, J. *Macromolecules* **2010**, *43*, 10498-10504.

(51) Castagna, A. M.; Wang, W.; Winey, K. I.; Runt, J. *Macromolecules* **2011**, *44*, 2791-2798.

(52) Kremer, F.; Schönhals, A. *Broadband Dielectric Spectroscopy*; Springer-Verlag: New York, 2002.

(53) The EP process was fit with a simple power law because the slope on the high-frequency side of EP is nearly identical to that of a simpler power law. This reduces the number of overall fitting parameters and achieves more stable fits. This method has been utilized previously to analyze relaxation processes of ionomers with rather good success.[46, 48, 49].

(54) In order to reduce the number of overall fitting parameters and to achieve more stable fits, we set the HN shape parameters (a and b) for the MWS process to the Cole-Cole type ($0 < a < 1$ and $b = 1$) in the fit of derivative spectra.

(55) Angell, C. A. *Chem. Rev.* **1990**, *90*, 523-542.

(56) The three data points at lower temperatures for p15ImBr are not included in the VFT fit. The semi-crystalline p15ImBr shows a transition in ω_{max} at T_m: above T_m the temperature dependence is well described by a single VFT expression, but below T_m it deviates. As a result, the T_g from extrapolation to 100 s is from the amorphous state.

(57) Angell, C. A. *Science* **1995**, *267*, 1924-1935.

(58) Mijović, J.; Sy, J.-W. *Macromolecules* **2002**, *35*, 6370-6376.

(59) Kanchanasopa, M.; Runt, J. *Macromolecules* **2004**, *37*, 863-871.

(60) Ngai, K. L.; Roland, C. M. *Macromolecules* **1993**, *26*, 2688-2690.

(61) Sayre, J. A.; Swanson, S. R.; Boyd, R. H. *J. Polym. Sci. Pol. Phys.* **1978**, *16*, 1739-1759.

(62) Onsager, L. *J. Am. Chem. Soc.* **1936**, *58*, 1486-1493.

(63) van Krevelen, D. W. *Properties of Polymers*; Elsevier: New York, 1990.

(64) Wang, W.; Tudryn, G. J.; Colby, R. H.; Winey, K. I. *J. Am. Chem. Soc.* **2011**, *133*,

10826-10831.

(65) Liu, W.; Janik, M. J.; Colby, R. H. In *Polymers for Energy Storage and Delivery: Polyelectrolytes for Batteries and Fuel Cells*; Page, K. A., Soles, C. L., Runt, J., Eds.; American Chemical Society: Washington, 2011, p 19-44.

(66) Kirkwood, J. G. *J. Chem. Phys.* **1939**, *7*, 911-919.

(67) Oster, G.; Kirkwood, J. G. *J. Chem. Phys.* **1943**, *11*, 175-178.

(68) Fröhlich, H. *Theory of Dielectrics : Dielectric Constant and Dielectric Loss*; Oxford : Clarendon Press: London, 1949.

(69) Soccio, M.; Choi, U. H.; Middleton, L. R.; Buitrago, C. F.; Masser, H. Q.; Cordaro, J.; Winey, K. I.; Runt, J. *Manuscript in preparation*.

(70) *Dielectric Properties of Heterogeneous Materials*; Priou, A., Ed.; Elsevier: New York, 1992.

For Table of Contents Use Only

Dynamics of Precise Ethylene Ionomers Containing Ionic Liquid Functionality

U Hyeok Choi,[1,2] L. Robert Middleton,[3] Michelina Soccio,[1] C. Francisco Buitrago,[4] Brian S. Aitken,[5] Hanqing Masser,[1,#] Kenneth B. Wagener,[5] Karen I. Winey,[3,4] and James Runt*[1]